Chemical Science

ROYAL SOCIETY OF CHEMISTRY

EDGE ARTICLE

View Article Online
View Journal | View Issue

Cite this: *Chem. Sci.*, 2024, **15**, 17979

All publication charges for this article have been paid for by the Royal Society of Chemistry

Received 22nd August 2024
Accepted 3rd October 2024

DOI: 10.1039/d4sc05632a

rsc.li/chemical-science

Revealing the overlithiation effect on cycling and calendar aging of a silicon/graphite electrode for high-energy lithium-ion batteries†

Xiaohong Wang, Chunhao Li, Shiyu Liu and Yongming Sun *

Lithium (Li) plating, triggered by fast charging and low temperature, will cause performance degradation and safety concerns for lithium-ion batteries (LIBs). However, strategically limited and controlled Li deposition might be advantageous for enhancing energy density. The detailed mechanism and regulation for performance improvement are yet to be fully explored. This study meticulously modulates the overlithiation capacity to regulate Li plating and probes its effects on the stability of high-capacity silicon/graphite (Si/Gr) electrodes through consecutive cycling and over the calendar aging period. The Si/Gr electrode (20 wt% Si) with a 20% overlithiation degree exhibits enhanced reversible capacity in comparison to the pristine Si/Gr electrode. This improvement is attributed to precision-controlled Li deposition, the increased electrochemical utilization of Si and Gr above 0 V, and the additional intercalation/alloying reactions below 0 V, which decelerate the progression of capacity degradation and significantly boost the electrochemical performance of Si/Gr electrodes. Moreover, this tailored Si/Gr electrode with a 20% overlithiation degree attenuates the deterioration associated with calendar aging. This research not only elucidates the intricate interplay and mechanisms of Li plating on Si/Gr electrodes during overlithiation but also presents a new understanding and approach to advance the performance of LIBs and extend their service lifespan.

1. Introduction

Lithium-ion batteries (LIBs) continue to gain prominence in electric vehicles and portable electronics, underscoring the pressing need for batteries with superior energy density and an extended lifespan.[1,2] This urgent demand motivates researchers to innovate and improve the anode, a fundamental component of LIBs.[3] The silicon/graphite (Si/Gr) anode has particularly drawn considerable attention due to the exceptional theoretical capacity of Si, which synergizes with the intrinsic good stability of Gr.[4–6] However, this alliance is not devoid of challenges. One of the significant obstacles lies in the mismatch of the working potentials between Si (~0.4 V *vs.* Li/Li^+) and Gr (~0.2 V *vs.* Li/Li^+), which significantly contributes to the interplay between them.[7,8] The crosstalk of Li^+ ions in the Si/Gr electrode compromises the uniform distribution of Li^+ ions over an entire Si particle from the interior to the outer shell, thereby hindering the complete dealloying process. The accumulation of trapped Li^+ ions in Si particles leads to pressure build-up, which in turn interferes with the subsequent intercalation into Gr. The interaction of electrochemical and mechanical behaviours of Si and Gr within the Si/Gr electrode accelerates the capacity fade.[9] To overcome this issue, various strategies have been explored, encompassing the design of the material structure, enhancement of the hardness of Gr, and the adoption of alternative materials with elevated working voltages.[9–12] These approaches strive to harmonize the lithiation/delithiation processes between Si and Gr, thus mitigating electrochemical degradation and extending the battery's operational life.

In real-world applications, LIBs are subjected to a relentless decline known as calendar aging, a gradual yet inevitable capacity fade over time, even when the batteries are not actively undergoing charge/discharge cycles.[13–16] In particular, anodes composed of Si degenerate at a more precipitous rate in comparison to their pure Gr counterparts. This heightened susceptibility of Si is attributed to its pronounced chemical reactivity, the dynamic evolution of the solid electrolyte interphase (SEI), and the rampant cycling of deleterious hydrolytic HF.[17] While the impacts of these factors are widely acknowledged, the complex interplay between Si and Gr in accelerating the calendar aging process remains an intricate conundrum, which necessitates further investigation to elucidate the fundamental mechanisms and to develop strategies that enhance the longevity of batteries.

Additionally, Li plating, a phenomenon associated with special scenarios such as fast charging, low temperatures, and overcharging, is widely acknowledged as a catalyst for the

Wuhan National Laboratory for Optoelectronics, Huazhong University of Science and Technology, Wuhan 430074, China. E-mail: yongmingsun@hust.edu.cn

† Electronic supplementary information (ESI) available. See DOI: https://doi.org/10.1039/d4sc05632a

degradation of LIBs.[18–20] The innovative application of "Gr/Li" hybrid anodes, which exploit continuous intercalation-plating mechanisms and feature regulated and uniform Li plating, has enabled batteries to achieve enhanced capacities.[21–24] These technological strides demonstrate that with careful management, Li deposition can be transformed from a perilous issue into a strategic advantage in the pursuit of amplifying energy densities, while suppressing its hazard effect. Despite these advancements, the precise effect of Li plating on the efficacy of the Si/Gr electrode remains unclear.

This study delves into the interrelationship between the overlithiation degree and the electrochemical behaviours of Si/Gr electrodes during regular cycling operation and throughout calendar aging. The Si/Gr electrode set at a 20% overlithiation degree exhibits enhanced electrochemical performance. However, an excessive overlithiation degree can induce uncontrolled Li plating, compromising overall stability and resulting in premature deactivation. Through the meticulous dissection of delithiation curves and a detailed analysis of dQ/dV profiles, we quantitatively discern the individual contributions of Li, Gr and Si and shed light on the mechanism of capacity optimization. Moreover, the Si/Gr electrode with a 20% overlithiation degree demonstrates improved capacity retention after calendar aging, outperforming the pristine Si/Gr electrode. By tracking the capacity changes of Li, Gr, and Si, we reveal the essential causes of the capacity degradation associated with calendar aging. Comprehensive surface examinations and evaluations of kinetic performance through an array of tests further enrich our understanding. Our findings provide new insights into the overlithiation effects on the Si/Gr electrode, contributing to the development of advanced LIBs with high energy density and prolonged calendar life.

2. Experimental section

2.1 Preparation of Si/Gr electrodes

The Si/Gr electrode was prepared *via* a slurry approach. The active material (80 wt% Gr and 20 wt% Si), carbon black (CB) and polyacrylic acid (PAA) in a mass ratio of 90 : 5 : 5 were evenly dispersed in *N*-methyl-2-pyrrolidone (NMP) to produce a uniform slurry. This resultant slurry was coated onto copper foil, subjected to a drying process at 80 °C for 12 h under vacuum, and then cut into discs with a diameter of 10 mm. The final Si/Gr electrode was designed to achieve a mass loading of ~3 mg cm^{-2}.

2.2 Electrochemical tests

The assembly of all cells was carried out in an argon-filled glove box (H_2O and O_2 < 1 ppm). The procedure involved integrating the pre-fabricated working electrode with Li metal foil serving as the counter electrode. They were separated with a polypropylene film and immersed in a specially formulated electrolyte. This electrolyte was a solution of 1 M $LiPF_6$, dissolved in a composite solvent comprising ethylene carbonate (EC), ethyl methyl carbonate (EMC), diethyl carbonate (DEC), and fluoroethylene carbonate (FEC) in a volumetric ratio of 3 : 3 : 7 : 1. Galvanostatic cycling was performed using a Land battery testing system. A complete charge–discharge protocol involved discharging to 0 V, followed by continuous discharging towards the designed overlithiation capacity, culminating with a charge back to 1.0 V. The overlithiation process was consistently applied to every cycle. Before calendar aging experiments, the cells underwent a formation process consisting of three cycles at 0.1C (1C = 900 mA h g^{-1}), followed by calendar storage at controlled temperatures of 30 or 60 °C for 145 h, and concluded with three additional cycles at 0.1C. Galvanostatic intermittent titration technique (GITT) measurements were conducted with a current pulse of 10 min at 0.1C, followed by a rest period of 3 h. Cyclic voltammetry (CV) tests were performed on a Biologic VMP3 electrochemical workstation with scan rates ranging from 0.01 to 0.1 mV s^{-1}. Electrochemical impedance spectroscopy (EIS) curves were collected over a frequency region of 10 mHz to 100 kHz with an amplitude of 10 mV.

2.3 Characterization

The morphological features and interphase compositions of electrodes were characterized using scanning electron microscopy (SEM, Nova NanoSEM 450) and X-ray photoelectron spectroscopy (XPS, Thermo Fisher ESCALAB 250Xi) measurements. The cycled electrodes were carefully washed with dimethyl carbonate (DMC) before the characterization.

3. Results and discussion

In our study, half cells were constructed for the overlithiation regulation of a Si/Gr electrode, which employed Li metal foil as the counter electrode. These half cells were methodically discharged (lithiated) to 0 V, followed by a continuous discharge to achieve predetermined overlithiation capacities of 180, 360, 540, and 720 mA h g^{-1} (the capacity was calculated based on the masses of Si and Gr unless otherwise stated), corresponding to 20%, 40%, 60%, and 80% overlithiation degrees, respectively. The discharge process is completed upon reaching the pre-set overlithiation capacity (<0 V). Subsequently, the cells were charged to 1 V at 0.5C after three cycles at 0.1C. The selected current density of 0.5C in a long-term cycling test aims to eliminate effects induced by fast charging and to simplify the variables, thus allowing for a clear assessment of Li plating.[18,25] As the overlithiation degree escalates from 0% to 80%, there is a distinct upsurge in overall charge capacity; however, there is a significant decline in stability and coulombic efficiency (CE) (Fig. 1A and S1†). We dissect the galvanostatic charge curve to ascertain the individual contributions of Li, Gr, and Si. The voltage span from 0.25 V to 1.0 V primarily pertains to the dealloying process of Li_xSi, and the voltage region from 0.1 V to 0.25 V is predominantly linked to the deintercalation of Li_xGr (Fig. 1C).[26] The utilization of FEC as an electrolyte additive effectively diminishes the Li stripping potential.[27,28] During the 100th cycle, a pronounced Li stripping plateau at ~0.06 V is observed in the Si/Gr electrode with a 20% overlithiation degree (marked as the Si/Gr-OL-20% electrode), a feature missing in the Si/Gr electrode without overlithiation (labelled as the Si/Gr-

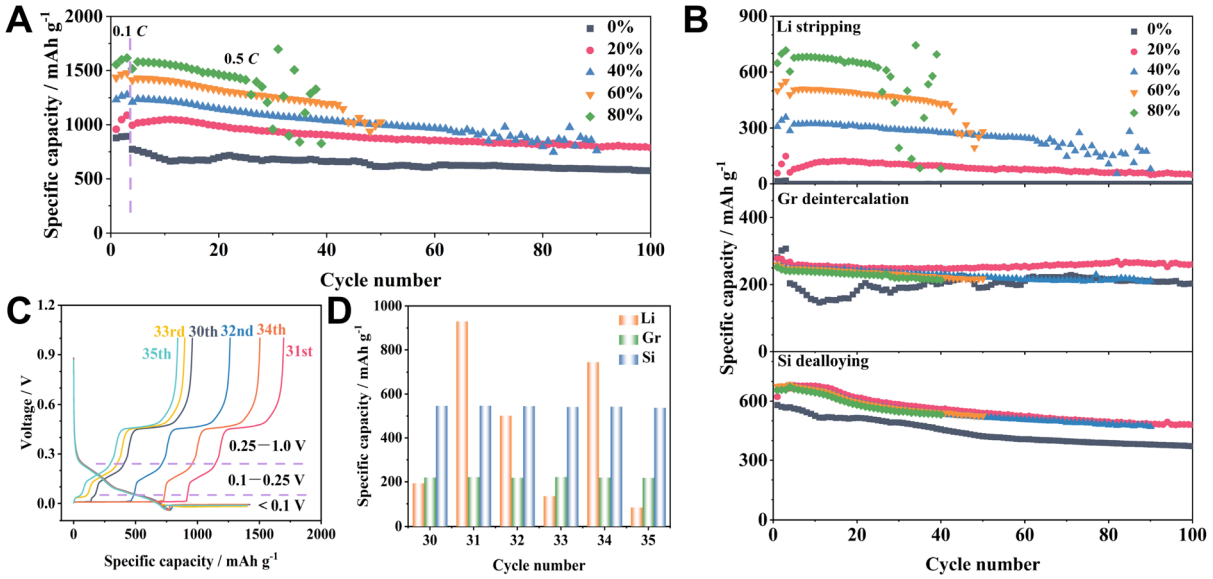

Fig. 1 Electrochemical performance of Si/Gr electrodes with varied overlithiation degrees. (A) Reversible delithiation capacity and (B) individual capacity contributions from Li stripping, Gr deintercalation, and Si dealloying processes of Si/Gr electrodes with overlithiation degrees from 0% to 80%. (C) Charge–discharge profiles and (D) delithiation capacities assigned to Li, Gr and Si of the Si/Gr electrode with an 80% overlithiation degree for the 30th to 35th cycles.

OL-0% electrode) (Fig. S2†). The voltage region below 0.1 V is delineated as the domain for the Li stripping behaviour. When the degree of overlithiation increases from 0 to 20%, there is a noticeable enhancement in the delithiation capacities of Si (0.25–1.0 V) and Gr (0.1–0.25 V) after 100 cycles: the capacity of Si climbs from 1854.5 to 2396.5 mA h g^{-1} (referencing to the Si mass) and that of Gr ascends from 254.1 to 325.9 mA h g^{-1} (based on the mass of Gr) (Fig. S3†). However, the growth of capacities deviates from a linear relationship in response to the intensifying overlithiation degree. During the overlithiation process, that is, the discharge process below 0 V, a dynamic competition emerges among the Li deposition, the intercalation of Gr, and the alloying with Si for the capture of Li^+ ions. At the initial stage of overlithiation (such as the overlithiation degree of 20%), the additional lithiation reactions below 0 V outpace Li plating. This phenomenon could be attributed to the abundance of unoccupied active sites, predominantly from the Si particles, which facilitate the alloying/intercalation reactions. When the overlithiation degree exceeds 20%, Li plating progressively emerges as the prevailing electrochemical reaction.[29] Therefore, the capacities for Li_xGr deintercalation and Li_xSi dealloying processes experience an increase with the overlithiation degree from 0% to 20% and then level off, maintaining stability despite further elevation of the overlithiation level up to 80% (Fig. 1B). In contrast, the Li stripping capacity (<0.1 V) exhibits a gradual increment, accompanied by a concurrent diminished stability as the overlithiation degree increases. The trend of Li stripping aligns with the behaviour of Si/Gr electrodes, emphasizing its pivotal role on the battery's electrochemical performance. The Si/Gr electrode with the highest overlithiation degree (80%) exhibits the least stability, lasting only ~20 cycles. A detailed analysis during its 30th to 35th cycles reveals dramatic fluctuations in Li stripping capacities compared to the minimal variations in the Li_xSi and Li_xGr delithiation capacities, suggesting erratic and incomplete Li stripping as the cause for impaired stability (Fig. 1C and D).[29] There is an abrupt escalation in Li stripping capacity to 929.3 mA h g^{-1} in the 31st cycle, even surpassing the designated overlithiation capacity of 720 mA h g^{-1}. The Cui group discovered that isolated Li metal can reestablish a connection with the electrode during subsequent Li plating processes.[30,31] The excessive Li stripping capacity in the 31st cycle can be ascribed to the reactivation of previously electrochemically inert "dead Li". In conclusion, its electrochemical performance is significantly enhanced through careful regulation of the overlithiation degree, demonstrating the advantage of meticulous management. The Si/Gr-OL-20% electrode exhibits 788 mA h g^{-1} (2.5 mA h cm^{-2}), maintaining a capacity retention of 79.2% after 100 cycles, which is superior to 575 mA h g^{-1} (1.8 mA h cm^{-2}, with a retention of 74.3%) of the Si/Gr-OL-0% electrode (Fig. S4†). On the other hand, an excessive overlithiation degree, represented by 80%, triggers uncontrolled Li deposition along with inadequate Li stripping, resulting in diminished stability. Therefore, diligently managing the trade-off between capacity and stability is crucial for optimizing the electrochemical performance.

A thorough exploration is essential to elucidate the electrochemical behaviour observed in the over-discharged Si/Gr electrodes. Typically, Si/Gr-OL-0% and Si/Gr-OL-20% electrodes during the 10th cycle deliver total charge capacities of 685.5 and 1066.9 mA h g^{-1}, respectively (Fig. 2A). The significant increment of 381.4 mA h g^{-1} exceeds the preassigned overlithiation capacity of 180 mA h g^{-1}. The residual enhancement can be traced back to the augmented lithiation capacity above 0 V (Fig. 2B). The Si/Gr-OL-20% electrode recorded at 886.9 mA h g^{-1} (>0 V) significantly outperforms that of the Si/Gr-

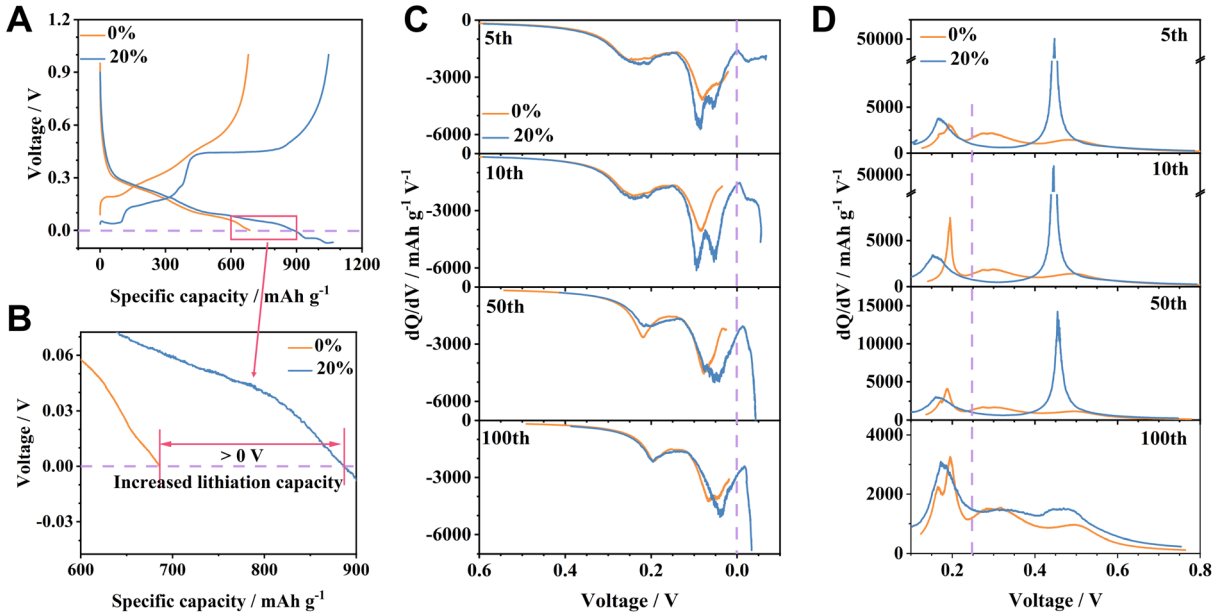

Fig. 2 Analysis of the effect of overdischarge on the electrochemical responses of Si and Gr in Si/Gr electrodes. (A) Galvanostatic charge–discharge curves and (B) their magnified profiles of Si/Gr-OL-0% and Si/Gr-OL-20% electrodes during the 10th cycle. dQ/dV curves during (C) lithiation and (D) delithiation processes for different cycles.

OL-0% electrode in the 10th cycle. The aforementioned elevated reversible capacity (381.4 mA h g^{-1}) partially arises from a boosted lithiation capacity (201.4 mA h g^{-1}, >0 V), in conjunction with the intended overlithiation capacity (180 mA h g^{-1}, <0 V). A further differential capacity (dQ/dV) analysis reveals a discernible intensification of peak intensity within the 0.15–0 V region for the Si/Gr-OL-20% electrode, signifying an increased lithiation capacity above 0 V (Fig. 2C). During charging, the dQ/dV curves demonstrate that the Si dealloying commences at ~0.25 V (Fig. 2D), corroborating the appropriateness of the segmented charge curves previously delineated. Moreover, the charge curves of the Si/Gr-OL-20% electrode feature a distinct plateau at ~0.4 V, which correlates with the dealloying of crystalline $Li_{15}Si_4$ (c-$Li_{15}Si_4$), as further described by the associated dQ/dV profiles (Fig. 2D).[32,33] The pronounced improvement of the c-$Li_{15}Si_4$ phase is due to the deepening alloying degree, stemming from the continuous alloying reactions below 0 V. This observed behaviour is consistent with the results from our prior research, suggesting that a meticulously executed overlithiation strategy can markedly enhance the formation of c-$Li_{15}Si_4$.[29] The intensity decay of this peak in subsequent cycles is attributable to the gradual deactivation of Si particles.[34]

In practical applications, the electrochemical performance of LIBs gradually deteriorates during both active service and periods of inactivity. A comprehensive assessment of the durability and longevity of LIBs necessitates examining the capacity fade associated with calendar aging. Our investigation specifically scrutinizes the impact of overlithiation on fully lithiated/delithiated Si/Gr-OL-0% and Si/Gr-OL-20% electrodes at static storage temperatures of 30 and 60 °C. Before storage experiments, each cell underwent three cycles to establish a stable SEI. Subsequently, the cell was discharged to 0 V at 0.1C to achieve a fully lithiated Si/Gr-OL-0% electrode. For the fully lithiated Si/Gr-OL-20% electrode, the cell was discharged at 0.1C past 0 V to attain the targeted overlithiation capacity of 180 mA h g^{-1}. Thereafter, all cells were stored at 60 °C for 145 h (Fig. 3A). The trajectory of open circuit voltage (OCV) exhibits an uptrend over the storage duration at 60 °C, with a more pronounced increase in the Si/Gr-OL-0% electrode (0.0145 V) as opposed to the Si/Gr-OL-20% electrode (0.0045 V) (Fig. 3B). For a detailed examination of the calendar aging effect on the lithiated electrode, the 3rd (before calendar storage), 4th (during storage), 5th (the first cycle after calendar storage), and 6th (the second cycle post-calendar storage) cycles are analysed (Fig. 3D). "C_{dn}" denotes the delithiation capacity at a certain cycle number "n", with "C_{d3}" referring to the delithiation capacity in the 3rd cycle before calendar storage. Capacity retention, labelled as "CR_{dn}", can be calculated using the formula $CR_{dn} = (C_{dn}/C_{d3}) \times 100\%$.[35] Without the influence of aging, the capacity retentions of the Si/Gr-OL-0% electrode for the 4th and 5th cycles are 99.8% and 99.2%, respectively (Fig. S5†). However, after calendar aging at 60 °C, the capacity retention significantly drops to 85.6% in the 4th cycle, which then rebounds to 95.0% in the 5th cycle and stabilizes at 94.1% in the 6th cycle (Fig. 3C). The slight reduction in the retention between the 5th and 6th cycles can primarily be attributed to substantial volumetric changes and ongoing interface side reactions during cycling.[34] The 4th cycle suffers from an overall capacity fade of 14.2%, which includes both irreversible and reversible losses. The 5th cycle exhibits a capacity fade of 4.2%, indicative of complete irreversibility. The segmented delithiation capacity is utilized to investigate the degradation mechanisms associated with calendar aging (Fig. 3E). The deintercalation capacity of Gr (0.1–0.25 V) in the Si/Gr-OL-0% electrode sharply declines from 286 mA h g^{-1} (3rd cycle) to

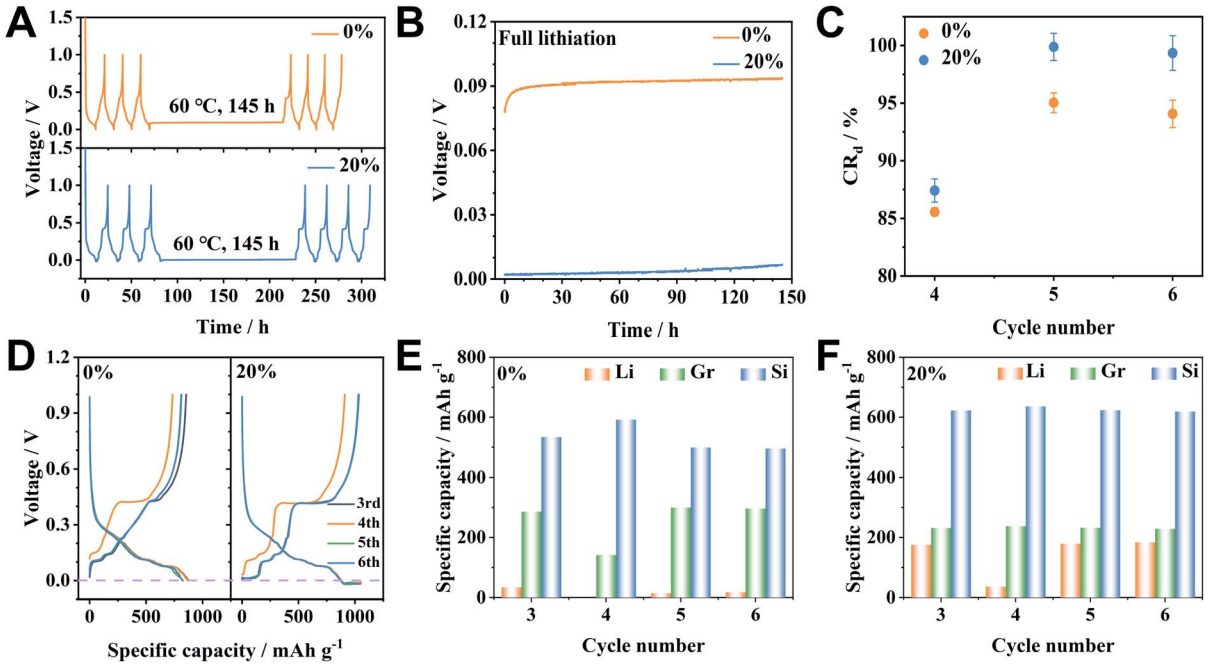

Fig. 3 Effect of overlithiation on lithiated Si/Gr-OL-0% and Si/Gr-OL-20% electrodes with calendar aging at 60 °C. (A) Voltage variations, (B) time-dependent OCV profiles, (C) capacity retention, and (D) voltage–capacity curves of lithiated Si/Gr-OL-0% and Si/Gr-OL-20% electrodes. Fluctuations in the Li stripping, Gr deintercalation, and Si dealloying capacities of lithiated (E) Si/Gr-OL-0% and (F) Si/Gr-OL-20% electrodes before and after the aging process.

141.6 mA h g^{-1} (4th cycle) and rebounds to 299.8 mA h g^{-1} (5th cycle) and 296.4 mA h g^{-1} (6th cycle). Simultaneously, the dealloying capacity of Si (0.25–1.0 V) surges from 534.2 mA h g^{-1} (3rd cycle) to 592.2 mA h g^{-1} (4th cycle), and then declines to 499.1 mA h g^{-1} (5th cycle) and 495.9 mA h g^{-1} (6th cycle). The incomplete recovery of the delithiation capacity of Si suggests irreversible attenuations, predominantly attributable to the inactivation of some Si particles.[36,37] The Si/Gr-OL-20% electrode also exhibits a decreased delithiation capacity with a retention of 87.4% in the 4th cycle after calendar aging (Fig. 3C). The negligible decline in the capacity retention in the 5th (99.9%) and 6th cycles (99.3%) indicates that the aging-deduced capacity reduction in the 4th cycle for the Si/Gr-OL-20% electrode may be largely reversible. Before calendar aging, the segmented delithiation capacities of the Si/Gr-OL-20% electrode are recorded as 175.6 mA h g^{-1} (Li, <0.1 V), 231.9 mA h g^{-1} (Gr, 0.1–0.25 V), and 622.8 mA h g^{-1} (Si, 0.25–1.0 V) in the 3rd cycle. These values after calendar storage shift to 36, 237.5, and 636.2 mA h g^{-1} in the 4th cycle, respectively. They rebound to 179.1, 232.6, and 623.6 mA h g^{-1} in the 5th cycle and maintain stability at 183.7, 229.2 and 619 mA h g^{-1} in the 6th cycle (Fig. 3F). The marked decline in Li stripping between the 3rd and 4th cycles could be attributed to the dissolution of Li metal, which is largely recoverable.[38] The rise in dealloying capacity points to ongoing alloying reactions during the aging period, as evidenced by a strengthened delithiation plateau at around 0.4 V, which is indicative of an intensified dealloying process of c-$Li_{15}Si_4$ (Fig. 3D). Relative to the Si/Gr-OL-0% electrode, the diminished capacity of Gr in the Si/Gr-OL-20% electrode can be ascribed to the increased mechanical pressure exerted by Si.[9] The delithiated Si/Gr-OL-0% electrode after calendar aging experiences a capacity reduction, a fading that is predominantly irreversible (Fig. S6†). The capacity loss in delithiated Si/Gr-OL-20% electrodes is attributed to the dissolution of Li metal (recoverable) and the deactivation of Si (unrecoverable). Moreover, the degradation behaviours of Si/Gr-OL-0% and Si/Gr-OL-20% electrodes at 30 °C demonstrate similarities to those at 60 °C (Fig. S7†). The calendar aging effects are markedly more severe at 60 °C, highlighting the temperature-dependent nature.[39] We also conducted aging experiments on pure lithiated/delithiated Si electrodes with 0% and 20% over-lithiation degrees at 60 °C for 145 h (Fig. S8†). The results obtained from Si electrodes are consistent with those observed on Si/Gr electrodes, where the electrode with a 20% over-lithiation degree exhibits enhanced capacity retention. The meticulous application of controlled overlithiation can potentially bolster the electrochemical endurance and stability, demonstrating the efficacy of this approach in improving the longevity and functional reliability of Si-based LIBs.

XPS measurements were performed to explore the surface composition evolution of the Si/Gr electrode subjected to calendar aging at 60 °C. Remarkable alterations can be detected in the high-resolution C 1s XPS spectra (Fig. 4A and B), with an elevated carbon content for lithiated Si/Gr-OL-20% electrodes compared to Si/Gr-OL-0% electrodes. This could be attributed to the SEI formation on the deposited Li metal.[40,41] The relative contents of organic (C–O (~286 eV) and C=O (~288.5 eV)) and inorganic (LiF (~684.5 eV), $Li_xPO_yF_z$ (~686.5 eV), and Li_2CO_3 (~289 eV)) species are normalized (Fig. 4C).[35,42] After calendar aging, an increased concentration of organic constituents is

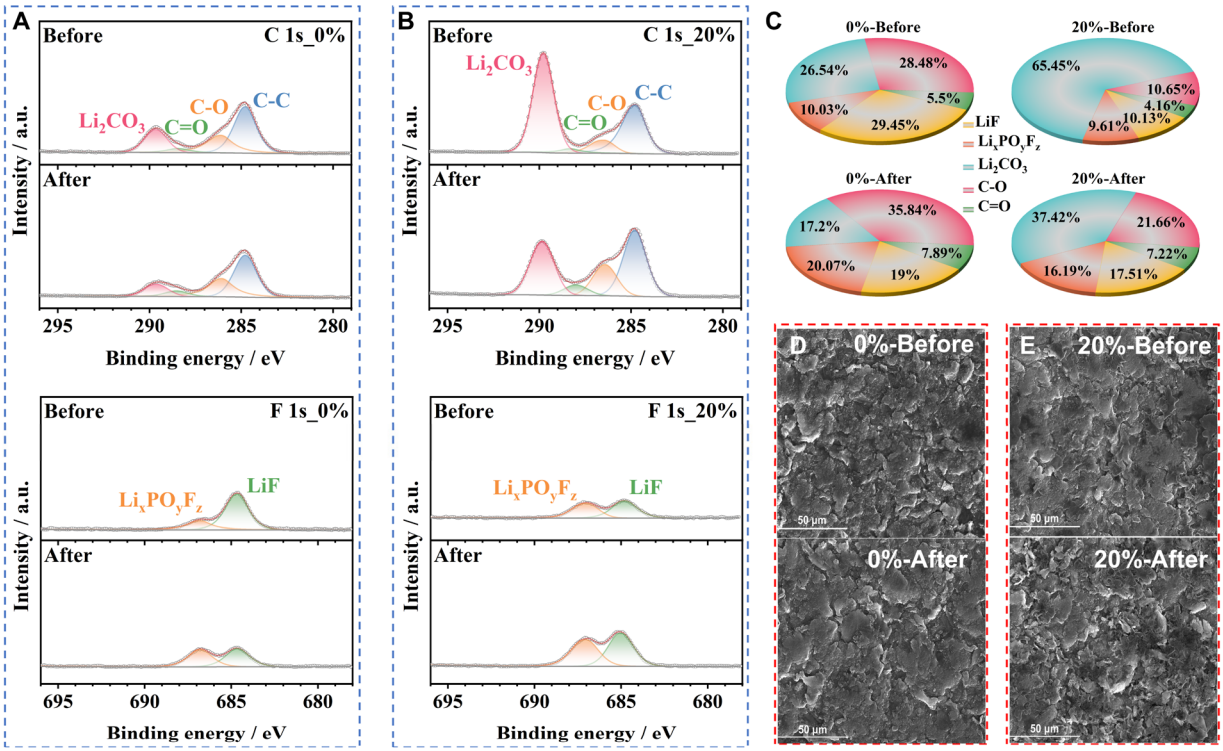

Fig. 4 Interface composition and morphology characterization of lithiated Si/Gr electrodes before and after calendar aging at 60 °C. C 1s and F 1s XPS spectra of the lithiated (A) Si/Gr-OL-0% and (B) Si/Gr-OL-20% electrodes. (C) Variations in the normalized relative contents of organic and inorganic components according to the XPS results. SEM images of the lithiated (D) Si/Gr-OL-0% and (E) Si/Gr-OL-20% electrodes.

detected, stemming from the decomposition of electrolyte components such as ethylene carbonate (EC) and fluoroethylene carbonate (FEC).[43] The aged, lithiated Si/Gr-OL-0% electrodes, with an organic-rich SEI, become porous and unstable.[40] The decline in LiF content observed in the Si/Gr-OL-0% electrode after calendar aging may be attributed to the dissolution of LiF.[44,45] Meanwhile, there is a conspicuous decrease in the amount of Li_2CO_3, accompanied by an increase in the content of $Li_xPO_yF_z$. These changes can be ascribed to the reduction of $LiPF_6$, catalyzed by trace water, yielding LiF, $Li_xPO_yF_z$, and HF.[46,47] HF reacts with Li_2CO_3, diminishing the amount of Li_2CO_3. Moreover, HF interacts with oxide-containing Si species (*e.g.*, SiO_2), generating additional water that could further instigate the hydrolysis of $LiPF_6$.[17] Additionally, side reactions between HF and Si incapacitate the active anode material as demonstrated by Ha *et al.*, where a mere 50 ppm of water can trigger a domino effect of pitting reactions on Si wafers.[48] Therefore, the Si degradation plays an important role in the irreversible capacity loss, which could deliver a lower stability than Gr. Independent of the aging and overlithiation conditions, lithiated Si/Gr electrodes exhibit a reduced prevalence of LiF and $Li_xPO_yF_z$ in contrast to their delithiated counterparts (Fig. S9A–C†). Delithiated Si/Gr-OL-0% electrodes show a more significant accumulation of LiF and $Li_xPO_yF_z$ compared to Si/Gr-OL-20% electrodes. The morphological SEM images reveal that although the lithiated Si/Gr electrode appears roughened, its surface integrity is preserved after calendar aging (Fig. 4D and E). In contrast, the SEM images show substantial cracking on delithiated Si/Gr electrodes, with aging treatment exacerbating the damage (Fig. S9D and E†). The decomposition of the electrolyte and the ensuing morphological evolution contribute to the increased interface impedance (Fig. S10†).

The Li^+ ion diffusion is inherently connected to the electrochemical performance, and this relationship is particularly crucial when evaluating the influence of overlithiation on the Si/Gr electrode. The GITT technique sheds light on the kinetic properties of the Si/Gr electrode (Fig. 5A).[49,50] No significant fluctuations are observed in either the apparent diffusion coefficient (D) of Li^+ ions or the overpotential for Si/Gr-OL-0% and Si/Gr-OL-20% electrodes throughout the lithiation process (Fig. 5B). During the delithiation process, within the voltage span of 0.2–0.4 V, the Si/Gr-OL-0% electrode presents a higher overpotential and reduced D values compared to the Si/Gr-OL-20% electrode (Fig. 5C). Moreover, the Si/Gr-OL-20% electrode exhibits an augmented hysteresis voltage in the 50–100% state of discharge (SOD) region, which can be ascribed to the enhanced formation of c-$Li_{15}Si_4$.[29] For a more detailed understanding of Li^+ ion diffusion, CV tests were conducted. The current peak at ~0.03 V is assigned to the Li stripping. Peaks A1, A2, C1, and C2 are associated with the intercalation and deintercalation of Gr, and peaks A3, A4, C3, and C4 are indicative of the alloying and dealloying processes of Si (Fig. 5D). The C4 peak at ~0.4 V is a signature of the c-$Li_{15}Si_4$ dealloying reaction,[32,33] with a notable amplification in peak intensity suggesting the high utilization ratio of Si. These peak currents are

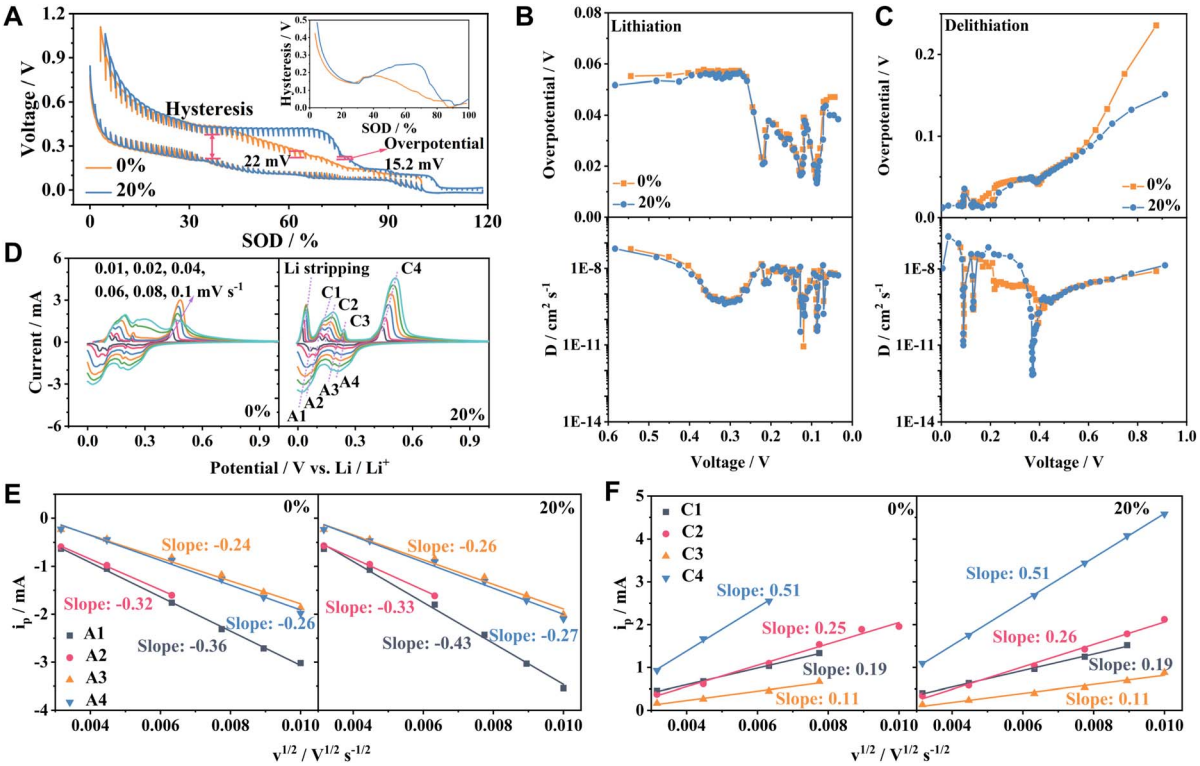

Fig. 5 Kinetic measurement of Si/Gr-OL-0% and Si/Gr-OL-20% electrodes. (A) Voltage response *versus* SOD in GITT tests; inset details the relationship of hysteresis voltage and SOD. Overpotential and *D* during (B) lithiation and (C) delithiation processes. (D) CV profiles of Si/Gr-OL-0% and Si/Gr-OL-20% electrodes. (E) Corresponding anodic peaks (A1, A2, A3, and A4) and (F) cathodic peaks (C1, C2, C3, and C4) with respect to the square root of the scan rate ($v^{1/2}$).

linearly proportional to the square root of the scan rate ($v^{1/2}$) (Fig. 5E and F). *D* can be quantified using the reaction $i_p = 2.69 \times 10^5 An^{3/2}C_0D^{1/2}v^{1/2}$,[49–51] where i_p refers to the peak current, *A* to the electrode's area, *n* to the number of electrons involved in the transfer, and C_0 to the Li^+ ion concentration. Given that these parameters—*A*, *n*, and C_0—are constants, *D* is determined from the slope of i_p *versus* $v^{1/2}$. Slopes for the Si/Gr-OL-0% and Si/Gr-OL-20% electrodes are found to be remarkably consistent, indicating that moderate overlithiation operation does not impede the diffusion of Li^+ ions. However, the unvarying *D* at ~0.4 V inferred from the CV test diverges from the finding of the GITT method. The GITT is found to be less suitable for determining *D* in a region where two distinct phases coexist.[52] The simultaneous existence of c-$Li_{15}Si_4$ and amorphous Li_xSi compromises the accuracy of *D* at ~0.4 V.

4. Conclusions

We have conducted a precise regulation of overlithiation capacity (degrees) to scrutinize its influence on a Si/Gr electrode during cyclic operation and calendar aging. A regulated overlithiation degree significantly enhances reversible capacity and cycling stability, whereas an excessive overlithiation degree could cause uncontrollable Li plating and the instability of the electrode. The increased reversible capacity of the Si/Gr-OL-20% electrode (788 mA h g^{-1} after 100 cycles) originates from the precisely managed Li deposition, the increased electrochemical utilization of Si and Gr above 0 V, and the continuous alloying/intercalation reaction below 0 V. After calendar aging, the fully lithiated Si/Gr-OL-20% electrode demonstrates enhanced capacity retention relative to the Si/Gr-OL-0% electrode. The capacity decay in lithiated electrodes comprises reversible and irreversible components. The permanent capacity loss is primarily attributable to the deactivation of Si particles. Furthermore, kinetic analysis reveals an accelerated Li^+ ion transport capability within the voltage range of 0.2–0.4 V during the delithiation of the Si/Gr-OL-20% electrode. The additional alloying reaction amplifies the formation of c-$Li_{15}Si_4$ and broadens the hysteresis voltage between lithiation and delithiation. This exhaustive research meticulously elucidates the intricate mechanisms of Si/Gr electrodes under operational and calendar aging conditions, establishing a foundation for their further refinement and paving the way for bolstering the electrochemical functionality.

Data availability

The data supporting this article have been included as part of the ESI.†

Author contributions

Xiaohong Wang: conceptualization, investigation, data curation, analysis, and writing – original draft. Chunhao Li and

Shiyu Liu: data curation. Yongming Sun: supervision, conceptualization, investigation, and writing – review and editing.

Conflicts of interest

There are no conflicts to declare.

Acknowledgements

This work is supported by the Natural Science Foundation of China (No. 52072137). The authors are grateful for the support provided by the Analytical and Testing Center of Huazhong University of Science and Technology.

References

1 K. T. Selvi, K. A. Mangai, J. A. Lett, I. Fatimah and S. Sagadevan, *J. Energy Storage*, 2024, **92**, 112208.
2 L. Sun, Y. Liu, L. Wang and Z. Jin, *Adv. Funct. Mater.*, 2024, 2403032.
3 X. Shen, X.-Q. Zhang, F. Ding, J.-Q. Huang, R. Xu, X. Chen, C. Yan, F.-Y. Su, C.-M. Chen, X. Liu and Q. Zhang, *Energy Mater. Adv.*, 2021, **2021**, 1205324.
4 X. Zhang, Z. Cui, E. Jo and A. Manthiram, *Energy Storage Mater.*, 2023, **56**, 562–571.
5 J. Zhang, D. Wang, R. Yuan, X. Li, J. Li, Z. Jiang, A. Li, X. Chen and H. Song, *Small*, 2023, **19**, 2207167.
6 P. Li, H. Kim, S.-T. Myung and Y.-K. Sun, *Energy Storage Mater.*, 2021, **35**, 550–576.
7 J. Kim, M.-H. Kim, Y. Kim, M. S. Kim, A. Choi, K.-M. Jeong and H.-W. Lee, *Energy Storage Mater.*, 2023, **57**, 269–276.
8 C. L. Berhaut, M. Mirolo, D. Z. Dominguez, I. Martens, S. Pouget, N. Herlin-Boime, M. Chandesris, S. Tardif, J. Drnec and S. Lyonnard, *Adv. Energy Mater.*, 2023, **13**, 2301874.
9 J. Moon, H. C. Lee, H. Jung, S. Wakita, S. Cho, J. Yoon, J. Lee, A. Ueda, B. Choi, S. Lee, K. Ito, Y. Kubo, A. C. Lim, J. G. Seo, J. Yoo, S. Lee, Y. Ham, W. Baek, Y.-G. Ryu and I. T. Han, *Nat. Commun.*, 2021, **12**, 2714.
10 Q. Sun, G. Zeng, J. Li, S. Wang, M. Botifoll, H. Wang, D. Li, F. Ji, J. Cheng, H. Shao, Y. Tian, J. Arbiol, A. Cabot and L. Ci, *Small*, 2023, **19**, 2302644.
11 J. Zhang, D. Wang, R. Yuan, X. Li, J. Li, Z. Jiang, A. Li, X. Chen and H. Song, *Small*, 2023, **19**, 2207167.
12 W. Zhang, S. Gui, W. Li, S. Tu, G. Li, Y. Zhang, Y. Sun, J. Xie, H. Zhou and H. Yang, *ACS Appl. Mater. Interfaces*, 2022, **14**, 51954–51964.
13 Y. Zhang, X. Li, E. Sivonxay, J. Wen, K. A. Persson, J. T. Vaughey, B. Key and F. Dogan, *Adv. Energy Mater.*, 2021, **11**, 2101820.
14 A. Chahbaz, F. Meishner, W. Li, C. Ünlübayir and D. U. Sauer, *Energy Storage Mater.*, 2021, **42**, 794–805.
15 J.-M. Kim, R. Yi, X. Cao, Y. Xu, Y. Xu, M. Engelhard, S. Tripathi, C. Wang and J.-G. Zhang, *ACS Energy Lett.*, 2024, **9**, 2318–2325.
16 J. Quinn, J.-M. Kim, R. Yi, J.-G. Zhang, J. Xiao and C. Wang, *Adv. Mater.*, 2024, **36**, 2402625.
17 J. D. McBrayer, M.-T. F. Rodrigues, M. C. Schulze, D. P. Abraham, C. A. Apblett, I. Bloom, G. M. Carroll, A. M. Colclasure, C. Fang, K. L. Harrison, G. Liu, S. D. Minteer, N. R. Neale, G. M. Veith, C. S. Johnson, J. T. Vaughey, A. K. Burrell and B. Cunningham, *Nat. Energy*, 2021, **6**, 866–872.
18 S. Liu, B. Gu, Z. Chen, R. Zhan, X. Wang, R. Feng and Y. Sun, *J. Energy Chem.*, 2024, **91**, 484–500.
19 J. Liu, Y. Zhang, J. Bai, L. Zhou and Z. Wang, *Electrochim. Acta*, 2023, **454**, 142362.
20 Z. M. Konz, B. M. Wirtz, A. Verma, T.-Y. Huang, H. K. Bergstrom, M. J. Crafton, D. E. Brown, E. J. McShane, A. M. Colclasure and B. D. McCloskey, *Nat. Energy*, 2023, **8**, 450–461.
21 C. Martin, M. Genovese, A. J. Louli, R. Weber and J. R. Dahn, *Joule*, 2020, **4**, 1296–1310.
22 Y. Liu, Y. Li, L. Chen, F. Yan, Z. Lin, J. Wang, J. Qiu, G. Cao, B. Wang and H. Zhang, *Energy Storage Mater.*, 2022, **53**, 621–628.
23 P. Shi, L.-P. Hou, C.-B. Jin, Y. Xiao, Y.-X. Yao, J. Xie, B.-Q. Li, X.-Q. Zhang and Q. Zhang, *J. Am. Chem. Soc.*, 2022, **144**, 212–218.
24 Z. Song, J. Xue, C. Wei, Q. Zhao, A. Zhou and J. Li, *Chem. Eng. J.*, 2024, **490**, 151618.
25 W. Mei, Y. Zhang, Y. Li, P. Zhuo, Y. Chu, Y. Chen, L. Jiang, H. Zhou, J. Sun and Q. Wang, *Energy Storage Mater.*, 2024, **66**, 103193.
26 C. Heubner, T. Liebmann, O. Lohrberg, S. Cangaz, S. Maletti and A. Michaelis, *Batteries Supercaps*, 2022, **5**, e202100182.
27 X.-Q. Zhang, X.-B. Cheng, X. Chen, C. Yan and Q. Zhang, *Adv. Funct. Mater.*, 2017, **27**, 1605989.
28 D. Weintz, S. P. Kühn, M. Winter and I. Cekic-Laskovic, *ACS Appl. Mater. Interfaces*, 2023, **15**, 53526–53532.
29 X. Wang, Y. Tan, W. Wang and Y. Sun, *ChemSusChem*, 2024, e202400971.
30 F. Liu, R. Xu, Y. Wu, D. T. Boyle, A. Yang, J. Xu, Y. Zhu, Y. Ye, Z. Yu, Z. Zhang, X. Xiao, W. Huang, H. Wang, H. Chen and Y. Cui, *Nature*, 2021, **600**, 659–663.
31 W. Zhang, P. Sayavong, X. Xiao, S. T. Oyakhire, S. B. Shuchi, R. A. Vilá, D. T. Boyle, S. C. Kim, M. S. Kim, S. E. Holmes, Y. Ye, D. Li, S. F. Bent and Y. Cui, *Nature*, 2024, **626**, 306–312.
32 M. N. Obrovac and L. J. Krause, *J. Electrochem. Soc.*, 2007, **154**, A103–A108.
33 Y. Li, Z. Cao, Y. Wang, L. Lv, J. Sun, W. Xiong, Q. Qu and H. Zheng, *ACS Energy Lett.*, 2023, **8**, 4193–4203.
34 A. Song, W. Zhang, H. Guo, L. Dong, T. Jin, C. Shen and K. Xie, *Adv. Energy Mater.*, 2023, **13**, 2301464.
35 Y. Zhang, W.-P. Wang, Y. Zhao, X. Zhang, H. Guo, H. Gao, D.-X. Xu, Y.-M. Zhao, G. Li, J.-Y. Liang, S. Xin and Y.-G. Guo, *Adv. Funct. Mater.*, 2023, **34**, 2310309.
36 N. Kirkaldy, M. A. Samieian, G. J. Offer, M. Marinescu and Y. Patel, *ACS Appl. Energy Mater.*, 2022, **5**, 13367–13376.
37 E. Moyassari, T. Roth, S. Kücher, C.-C. Chang, S.-C. Hou, F. B. Spingler and A. Jossen, *J. Electrochem. Soc.*, 2022, **169**, 010504.
38 A. B. Gunnarsdóttir, C. V. Amanchukwu, S. Menkin and C. P. Grey, *J. Am. Chem. Soc.*, 2020, **142**, 20814–20827.

39 M. Alipour, C. Ziebert, F. V. Conte and R. Kizilel, *Batteries*, 2020, **6**, 35.
40 Y. Liao, H. Zhang, Y. Peng, Y. Hu, J. Liang, Z. Gong, Y. Wei and Y. Yang, *Adv. Energy Mater.*, 2024, **14**, 2304295.
41 X. Cao, Y. Xu, L. Zou, J. Bao, Y. Chen, B. E. Matthews, J. Hu, X. He, M. H. Engelhard, C. Niu, B. W. Arey, C. Wang, J. Xiao, J. Liu, C. Wang, W. Xu and J.-G. Zhang, *Energy Environ. Sci.*, 2023, **16**, 1548–1559.
42 Y. Yang, Z. Yang, Z. Li, J. Wang, X. He and H. Zhao, *Adv. Energy Mater.*, 2023, **13**, 2302068.
43 J. M. Martinez de la Hoz, F. A. Soto and P. B. Balbuena, *J. Phys. Chem. C*, 2015, **119**, 7060–7068.
44 J. Jones, M. Anouti, M. Caillon-Caravanier, P. Willmann and D. Lemordant, *J. Mol. Liq.*, 2010, **153**, 146–152.
45 Y. Lu, Z. Tu and L. A. Archer, *Nat. Mater.*, 2014, **13**, 961–969.
46 M. Liu, J. Vatamanu, X. Chen, L. Xing, K. Xu and W. Li, *ACS Energy Lett.*, 2021, **6**, 2096–2102.
47 B. S. Parimalam and B. L. Lucht, *J. Electrochem. Soc.*, 2018, **165**, A251–A255.
48 Y. Ha, C. Stetson, S. P. Harvey, G. Teeter, B. J. T. d. Villers, C.-S. Jiang, M. Schnabel, P. Stradins, A. Burrell and S.-D. Han, *ACS Appl. Mater. Interfaces*, 2020, **12**, 49563–49573.
49 J. Wang and G. M. KoenigJr, *J. Electrochem. Soc.*, 2023, **170**, 050534.
50 X. Wang, L. Qi and H. Wang, *ACS Appl. Mater. Interfaces*, 2019, **11**, 30453–30459.
51 R. Zhan, S. Liu, W. Wang, Z. Chen, S. Tu, X. Wang, H. Ge, H. Luo, T. Chai, Y. Ou, Y. Tan and Y. Sun, *Mater. Horiz.*, 2023, **10**, 5246–5255.
52 K. Tang, X. Yu, J. Sun, H. Li and X. Huang, *Electrochim. Acta*, 2011, **56**, 4869–4875.